Conventional, Bayesian, and Modified Prony's methods for characterizing fast and slow waves in equine cancellous bone

Amber M. Groopman[a] and Jonathan I. Katz
Department of Physics, Washington University in St. Louis, St. Louis, Missouri 63130, USA

Mark R. Holland
Department of Radiology and Imaging Sciences, Indiana University-Purdue University School of Medicine, Indianapolis, Indiana 46202, USA

Fuminori Fujita and Mami Matsukawa
Laboratory of Ultrasonic Electronics, Research Center for Wave Electronics, Doshisha University, Kyotanabe, 610-0321 Kyoto, Japan

Katsunori Mizuno
Underwater Technology Research Center, The University of Tokyo, Meguro-ku, Tokyo 153-8505, Japan

Keith A. Wear
Center for Devices and Radiological Health, Food and Drug Administration, Silver Spring, Maryland 20993, USA

James G. Miller
Department of Physics, Washington University in St. Louis, St. Louis, Missouri 63130, USA

(Received 19 February 2015; revised 16 June 2015; accepted 21 June 2015; published online 5 August 2015)

Conventional, Bayesian, and the modified least-squares Prony's plus curve-fitting (MLSP + CF) methods were applied to data acquired using 1 MHz center frequency, broadband transducers on a single equine cancellous bone specimen that was systematically shortened from 11.8 mm down to 0.5 mm for a total of 24 sample thicknesses. Due to overlapping fast and slow waves, conventional analysis methods were restricted to data from sample thicknesses ranging from 11.8 mm to 6.0 mm. In contrast, Bayesian and MLSP + CF methods successfully separated fast and slow waves and provided reliable estimates of the ultrasonic properties of fast and slow waves for sample thicknesses ranging from 11.8 mm down to 3.5 mm. Comparisons of the three methods were carried out for phase velocity at the center frequency and the slope of the attenuation coefficient for the fast and slow waves. Good agreement among the three methods was also observed for average signal loss at the center frequency. The Bayesian and MLSP + CF approaches were able to separate the fast and slow waves and provide good estimates of the fast and slow wave properties even when the two wave modes overlapped in both time and frequency domains making conventional analysis methods unreliable. © *2015 Acoustical Society of America*. [http://dx.doi.org/10.1121/1.4923366]

[CCC] Pages: 594–604

I. INTRODUCTION

Due to its complex structure, which consists of a hard trabecular matrix interspersed with liquid bone marrow, cancellous bone permits the propagation of two longitudinal wave modes, referred to as fast waves and slow waves (Hosokawa and Otani, 1997, 1998). Based on Biot theory, the fast wave is thought to be generated by the solid and fluid components moving in phase, while the slow wave is generated by the solid and fluid components moving out of phase (Biot, 1956a,b; Haire and Langton, 1999; Fellah *et al.*, 2004). Observation of the two wave modes in the time-domain is very dependent on the angle of insonification relative to the main trabecular orientation. Previous studies have demonstrated that the speeds of sound of the fast and slow waves become more similar as the angle of insonification between the ultrasound beam and the predominant trabecular orientation approaches perpendicular alignment, thus, potentially causing the two wave modes to overlap substantially in the time-domain (Hosokawa and Otani, 1998; Hughes *et al.*, 2007; Lee *et al.*, 2007; Mizuno *et al.*, 2008; Hoffman *et al.*, 2012). We have previously demonstrated that applying conventional analysis methods to these mixed-mode signals can produce misleading wave properties, including negative dispersion (Marutyan *et al.*, 2006; Bauer *et al.*, 2008; Bauer *et al.*, 2009; Anderson *et al.*, 2010).

Successful separation and analysis of the individual fast and slow waves may bring about a better understanding of the physical mechanisms underlying the propagation of ultrasonic waves in cancellous bone, potentially leading to improvements in the diagnostic capabilities of clinical quantitative ultrasound devices. Over the past few years, several techniques have been introduced to identify and potentially

[a]Electronic mail: nelsonam@wustl.edu

 0001-4966/2015/138(2)/594/11/$30.00

isolate the fast and slow waves, including a space alternating generalized expectation maximization algorithm (Dencks *et al.*, 2009; Dencks and Schmitz, 2013), the modified least squares Prony's (MLSP) method (Wear, 2010), coded excitation (Lashkari *et al.*, 2012), the modified least squares Prony's plus curve-fitting (MLSP + CF) (Wear, 2013), band-limited deconvolution (Wear, 2014), and generalized harmonic analysis (Maruo and Hosokawa, 2014). We have previously demonstrated an approach utilizing Bayesian probability theory that is capable of isolating the fast and slow waves, even in cases of extreme overlap and interference (Marutyan *et al.*, 2007). This Bayesian technique has proven successful at separating the two wave modes in experimental data from plastic phantoms (Anderson *et al.*, 2010) and from cancellous bone (Nelson *et al.*, 2011; Hoffman *et al.*, 2012). However, in the previous studies using Bayesian methods on measurements of cancellous bone, the fast and slow waves overlapped in time and frequency domains, thus, not permitting the use of conventional analysis methods. Therefore, there was no appropriate standard for comparison with the Bayesian method available.

Fujita *et al.* (2013) performed through-transmission measurements on equine cancellous bone that was gradually and systematically shortened. Since the angle of insonification was parallel to the predominant trabecular orientation and the bone volume fraction of the specimen was quite high, the separation between the fast wave and slow wave velocities was rather large. In the present study, we analyzed data acquired in the same laboratory from a specimen adjacent to the specimen used to acquire the data presented in Fujita *et al.* (2013). In the current study, conventional, Bayesian, and MLSP + CF analysis techniques were employed to analyze the data over a wide range of sample thicknesses. The objective of the current study was to directly compare estimates for phase velocity and attenuation properties of fast and slow waves for the three methods in order to further validate the Bayesian and MLSP + CF approaches.

II. METHODS

A. Data acquisition

The data acquisition process has been described previously in Fujita *et al.* (2013). A brief overview will be given here. A single, rectangular, defatted cancellous bone specimen, ~22.4 mm × 22.4 mm × 11.8 mm in size, was extracted from the left radius of a 36-month-old horse. The sample was placed in an acoustic tube immersed in a room temperature tank filled with degassed water. A pair of planar, wideband polyvinylidene fluoride transducers, with active areas of 15 mm × 15 mm, was used to interrogate the sample in a through-transmission arrangement. The sample was oriented so that the propagation direction was parallel to the main trabecular alignment, which was confirmed by micro-CT measurements. The transducers were separated by a distance of 100 mm with the front surface of the sample positioned at 75 mm from the transmitting transducer.

The transmitter was excited by a single cycle of a 1 MHz sinusoidal pulse with a peak-to-peak amplitude of 5 V generated by a function generator (33250A, Agilent, CO) which was then amplified by 20 dB using a power amplifier (4055, NF Corporation, Kanagawa, Japan). The received signals, after passing through the sample, were digitized by an oscilloscope (TDS 524A, Tektronix Inc., OR) with a 20 dB preamplifier (5307, NF Corp., Kanagawa, Japan). This process was repeated as the equine sample was shortened from 11.8 mm down to 0.5 mm in increments of ~0.5 mm for a total of 24 data sets. At each step, the sample was ground down using a polishing machine (Speed Lap, Maruto, Tokyo, Japan).

B. Model of wave propagation in cancellous bone

In a through-transmission experiment, propagation through cancellous bone can be modeled as

$$\text{Output}(f) = \text{Input}(f)[H_{\text{fast}}(f) + H_{\text{slow}}(f)], \tag{1}$$

where $\text{Output}(f)$ and $\text{Input}(f)$ are the complex Fourier spectra of the model waveform and the transmitted ultrasonic signal, respectively. For experimentally acquired data, a reference water-path-only signal is used as the source for $\text{Input}(f)$. The transfer functions, $H_{\text{fast}}(f)$ and $H_{\text{slow}}(f)$, for the fast and slow waves can be described by

$$H_k(f) = A_k \exp[-\beta_k f d] \exp\left[\frac{i2\pi f d}{c_k(f)}\right], \tag{2}$$

where k stands for either fast or slow, A_k are the frequency-independent amplitudes of the two waves, β_k are the slopes of the attenuation coefficients, $c_k(f)$ are the phase velocities, and d is the sample thickness (Marutyan *et al.*, 2006; Anderson *et al.*, 2008, 2010). The parameters, A_k, are constrained to lie between 0 and 1, indicating that the amplitude of the fast and slow waves must be less than or equal to the amplitude of the reference (water-path-only) signal. In order to satisfy the causality-induced Kramers–Kronig relations, the phase velocities are related to the linear-with-frequency attenuation coefficients by

$$c_k(f) = c_k(f_0) + [c_k(f_0)]^2 \frac{\beta_k}{\pi^2} \ln\left(\frac{f}{f_0}\right), \tag{3}$$

where f_0 is a reference frequency within the experimental bandwidth, typically the nominal center frequency of the transmitting transducer (O'Donnell *et al.*, 1981; Waters *et al.*, 2003, 2005).

C. Bayesian parameter estimation

This method has been described in previous publications from our laboratory (Marutyan *et al.*, 2007; Anderson *et al.*, 2010; Nelson *et al.*, 2011; Hoffman *et al.*, 2012). Bayesian probability theory was used to estimate the six fast and slow wave ultrasonic parameters, $\{A_{\text{fast}}, A_{\text{slow}}, \beta_{\text{fast}}, \beta_{\text{slow}}, c_{\text{fast}}(f_0), c_{\text{slow}}(f_0)\}$, in the wave propagation model detailed above. The prior probabilities for each of the six parameters were assigned to be bounded Gaussian distributions with the characteristics listed in Table I, and f_0 was set to 1 MHz, the

TABLE I. Prior probability distributions for each model parameter. The means and standard deviations define Gaussian distributions that are bounded by the minimum and maximum values.

			β_{fast}	β_{slow}	c_{fast} (1 MHz)	c_{slow} (1 MHz)
	A_{fast}	A_{slow}	(dB/cm/MHz)		(m/s)	
Minimum	0	0	0	0	1500	1300
Mean	0.5	0.5	25	25	2000	1500
Maximum	1.0	1.0	50	50	2500	1700
Standard deviation	0.5	0.5	25	25	500	200

center frequency of the transmitted signal. Since the marginalized posterior probability distributions for each parameter are complicated five-dimensional integrals that are difficult or impossible to solve analytically, these integrals were approximated using Markov chain Monte Carlo simulation with simulated annealing. This Bayesian parameter analysis was performed on all 24 data sets acquired at sample lengths ranging from 11.8 mm down to 0.5 mm.

D. Conventional analysis

Conventional analysis was performed on the data from sample lengths that were sufficiently long as to permit enough separation of the fast and slow waves so that time-domain gating could be carried out effectively. A 90% Tukey window was used to time-gate the received sample signals into individual fast and slow waves for sample thickness from 6.0 mm to 11.8 mm, a total of 13 lengths.

In this analysis, the individually windowed fast waves and slow waves were compared to a reference signal obtained by recording a signal traveling only through water. The frequency-dependent phase velocities were determined using

$$c_k(\omega) = \frac{c_{ref}}{1 + \frac{c_{ref}\Delta\phi(\omega)}{\omega d}}, \tag{4}$$

where c_{ref} is the speed of sound in the reference medium and $\Delta\phi(\omega)$ is the difference in the unwrapped phases of the reference signal and the through-sample signals.

The attenuation coefficients, in units of dB/cm, of the time-gated fast waves and slow waves were determined using a log-spectral subtraction technique

$$\alpha_k(f) = \frac{1}{d}\left[10\log\left(|\tilde{V}_{ref}(f)|^2\right) - 10\log\left(|\tilde{V}_k(f)|^2\right) + 10\log\left(T^I_{ref\to k}T^I_{k\to ref}\right)\right], \tag{5}$$

where $|\tilde{V}_{ref}(f)|$ and $|\tilde{V}_k(f)|$ are the magnitudes of the Fourier transforms of the reference signal and the fast (or slow) signal, respectively, and $T^I_{ref\to k}$ and $T^I_{k\to ref}$ are the intensity transmission coefficients at the boundaries between the reference medium and the sample. The third term in Eq. (5) represents the losses occurring at the interfaces between the host medium and the sample as the wave propagates from the transmitter to the receiver. These insertion losses could, in principle, be determined by calculating the intensity transmission coefficients for the front wall interface and the back wall interface; however, this requires knowledge of the acoustic impedances of the fast and slow waves. Since the individual fast wave and slow wave impedances are unknown, an alternative method was employed. The insertion losses were estimated by determining the zero-frequency intercepts of the signal loss versus frequency curves. The normalized broadband ultrasound attenuations (nBUAs) of the fast and slow waves were determined by the slope of a linear fit to the attenuation coefficients over the bandwidth from 0.58 MHz to 1.25 MHz.

E. MLSP+CF method

The MLSP+CF method was also applied to the experimental data. This method has been described in a previous publication (Wear, 2013). Briefly, as with the Bayesian method, the frequency-domain signal was modeled as the sum of two components with attenuation coefficients that were linear-with-frequency and phase velocities with functional forms consistent with the Kramers–Kronig relations in order to ensure causality (O'Donnell *et al.*, 1981; Marutyan *et al.*, 2006, 2007). The MLSP method (Wear, 2010) was used to make rapid initial guesses for parameter values to be used as inputs to a curve-fitting routine. A six-dimensional parameter space (two amplitudes, two attenuation slopes, and two phase velocities) was searched in order to minimize mean square difference between data and the model function. The search algorithm was accelerated by exploiting correlations among search parameter estimates. The search space resolutions were 1 dB/cmMHz for attenuation slopes and 5 m/s for velocities. Frequency-domain data were analyzed over the range from 300 kHz to 1.5 MHz. This method has been shown to produce accurate estimates of attenuation slopes and phase velocities in simulations based on parameters reported in the literature for cancellous bone (Wear, 2013). In addition, it has been shown to be consistent with the broadband deconvolution method (Wear, 2014) for fast and slow wave detection in bovine cancellous bone (Wear *et al.*, 2014).

F. Estimation of apparent frequency

In Fujita *et al.* (2013), the apparent center frequencies of the fast waves and slow waves at each sample length were determined using time intervals of peaks and zero-crossings in the time-domain signals. As discussed in Nelson *et al.* (2011), time-domain analysis methods may be inappropriate for broadband ultrasonic wave propagation. Since the Bayesian probability theory technique can recover the individual fast and slow waves, it permits the spectral content of the individual fast and slow waves to be determined using frequency-domain methods. This analysis is useful for determining whether fast and slow waves that overlap in the time-domain also overlap in the frequency domain. (If not, the wave separation task is relatively straightforward.) The shifted center frequencies of the Bayesian-separated fast and slow waves were determined by calculating the centroid of the linear power

spectrum of the fast and slow waves at each sample thickness. (The centroid or center-of-mass was employed rather than the maximum value because the majority of the spectra were either asymmetric or contained multiple peaks of similar amplitude.) The experimental spectral shifts in frequency of the fast and slow waves were compared to the spectral shifts predicted by the theory of Ophir and Jaeger (1982). When a wideband ultrasonic pulse propagates through a lossy medium whose attenuation coefficient increases with frequency, the higher frequency components will be attenuated more than lower frequency components. This results in a downshift in the center frequency of the received power spectrum. In the case of a linear-with-frequency attenuation coefficient (Hosokawa and Otani, 1997; Njeh *et al.*, 1999; Laugier and Haïat, 2011), the spectral shift is given by

$$\Delta f = f_0 - f_c = 2\beta_k d\sigma^2, \tag{6}$$

where f_0 is the center frequency of the reference signal, f_c is the downshifted center frequency, β_k is the slope of the attenuation coefficient (nBUA), d is the propagation distance, and σ^2 is the variance of the spectrum of the transmitted pulse (Ophir and Jaeger, 1982). The predicted spectral shifts for the fast and slow waves were determined using Eq. (6) with $\sigma^2 = 0.08$ MHz^2, d being the sample thickness, and β_k being the Bayesian-estimated nBUA.

III. RESULTS

A. Radiofrequency data

The received signals that traveled through each of the sample thicknesses are shown in Fig. 1. Separated fast and slow waves are clearly evident at the larger sample thicknesses, ranging from 11.8 mm to 6 mm. Samples thinner than ~6 mm produced a sample signal that had either overlapping fast and slow waves or appeared to be only a single wave. The effects of sample thickness on the presence of fast and slow waves are more clearly observed in the right column of Fig. 1, in which the slow wave was normalized to unit amplitude for each trace. As the sample thickness decreased, the location of the fast wave moved closer to the location of the slow wave. The slow wave also shifted to earlier times as the sample thickness decreased.

B. Apparent frequency

The apparent frequencies of the fast and slow waves as determined by the centroids of the Bayesian-separated fast and slow waves are shown as functions of sample thickness in Fig. 2. The fast waves exhibited a rapid downshift in center frequency from the original center frequency of $f_0 = 1$ MHz with longer sample lengths. At the longest sample length ($d = 11.8$ mm), the downshifted center frequency of the fast wave was 507 kHz, which is approximately half of the center frequency of the reference signal. This behavior is consistent with the findings of Hasegawa *et al.* (2010) and Nagatani and Tachibana (2014), who found that the frequency of the fast wave dropped to 0.55 MHz or lower when the transmitted signal had a center frequency of 1 MHz. The slow waves also displayed a downshifted center frequency, although not as significant as the fast wave. At the longest sample thickness, the center frequency of the slow wave was ~814 kHz. The results of the (frequency-domain) centroid frequencies were compared to both the time-domain apparent frequencies, determined using the methods reported in Fujita *et al.* (2013), and the predicted center frequencies, f_c, determined by Eq. (6). The downshifted center frequencies determined by the centroid agreed well with the predicted apparent frequencies calculated using Eq. (6) at all thicknesses and with the time-domain-derived apparent frequency (Fujita *et al.*, 2013) for thicknesses of 4 mm and above, as shown in Fig. 2. These results support previous reports that

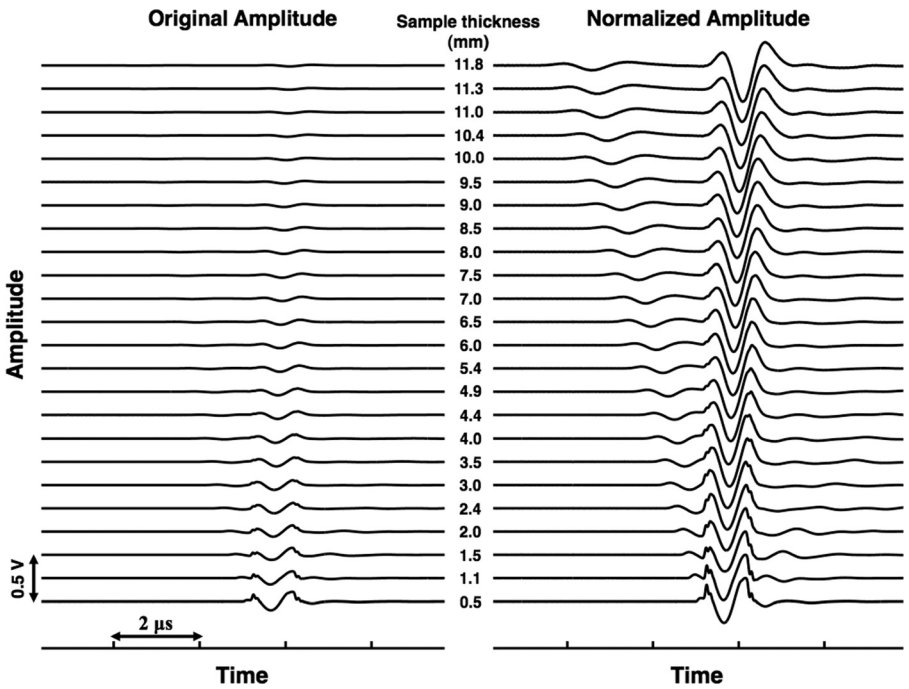

FIG. 1. Acquired radiofrequency signals transmitted through equine cancellous bone for 24 sample thicknesses ranging from 11.8 mm down to 0.5 mm. The right column magnifies the vertical scale of the left column by normalizing the maximum voltage to unity for each sample thickness, permitting the fast wave in the longer sample lengths to be visible.

the fast wave slope of attenuation (nBUA) is often greater than the slow wave slope of attenuation, thus, leading to the fast wave having a greater downshift in frequency than the slow wave (Hosokawa and Otani, 1997; Cardoso *et al.*, 2003; Waters and Hoffmeister, 2005).

Figure 2 shows that for the thinnest samples, where the wave separation was the most challenging, the centroids for fast and slow waves were near 1 MHz, indicating substantial overlap in the frequency domain, as well as the time-domain. A Gaussian fit to the source spectrum, proportional to $\exp[-(f-f_0)^2/2\sigma^2]$, yielded $\sigma = 283$ kHz, indicating substantial frequency-domain overlap when the difference between fast and slow centroids was <283 kHz. The difference between fast and slow centroids increased from near zero at small thicknesses to a maximum value of 307 kHz at a thickness $d = 11.8$ mm.

C. Separation using time gates

The phase velocities of the fast and slow waves, determined using conventional phase spectroscopy, for sample thickness ranging from 6.0 mm to 11.8 mm, all exhibited positive dispersion. A signal containing parts of both fast and slow waves might display negative dispersion when analyzed conventionally (Marutyan *et al.*, 2006; Anderson *et al.*, 2008, 2010; Bauer *et al.*, 2008). The fact that only positive dispersions were observed suggests, but does not prove, that sufficient separation of the fast and slow waves was achieved using time gating.

Figure 3 shows the average signal losses of the fast and slow waves as functions of frequency. The zero-frequency intercepts of the signal losses, which should correspond to the insertion losses, were subtracted from the signal loss curves to obtain the attenuation coefficients of the individual fast and slow waves. Additional evidence supporting good separation of the fast and slow waves using conventional techniques was that the attenuation coefficients of the separated fast waves and slow waves showed, approximately, a linear dependence with frequency over the usable bandwidth.

D. Bayesian estimation

In order to illustrate the results of Bayesian analysis, the experimental data and the model constructed from Bayesian parameter estimation are shown in Fig. 4 for four selected sample thicknesses. For a sample thickness of 1.1 mm, only one wave was apparent. For a thickness of 4.0 mm, the fast and slow waves were significantly overlapped. For a sample thickness of 7.0 mm, the fast and slow waves were just barely separated. For a thickness of 11.0 mm, the fast and slow waves were completely separated. The residuals, the difference between the experimental trace and the model trace, are shown in the middle panel of each subplot, and were scaled to be consistent with the overall amplitude of the experimental signal.

In order to quantify the goodness-of-fit between the Bayesian-generated model and the experimental signal, the coefficient of variation (CV) of the root-mean-square-deviation (RMSD) given by

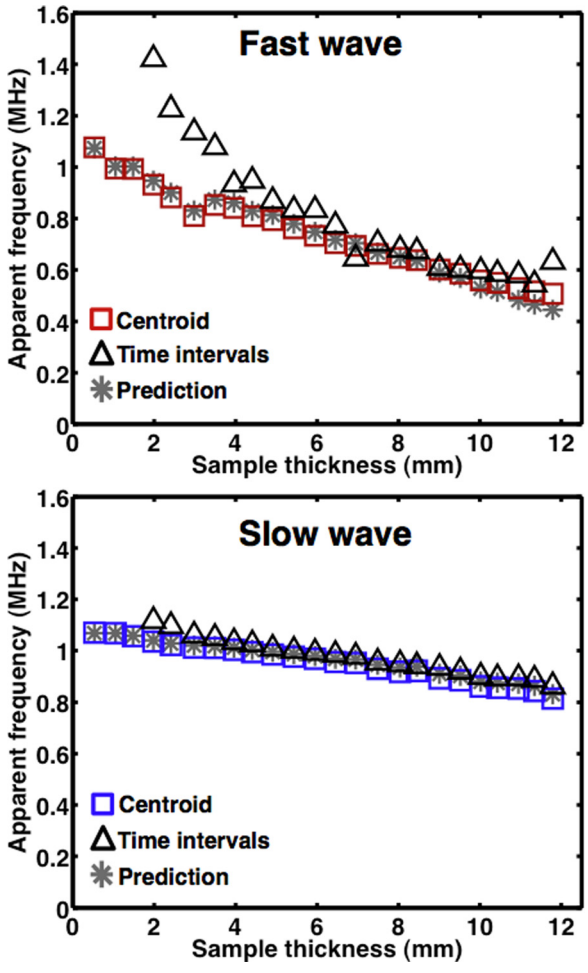

FIG. 2. (Color online) Comparison of the apparent frequencies of the fast waves and the slow waves using three methods. The squares show the shifting center frequencies of the two waves using the (frequency-domain) centroid of the Bayesian-separated fast and slow waves. The triangles represent the apparent frequency determined using time-domain methods described in Fujita *et al.* (2013). The stars represent the predicted center frequency determined using Eq. (6).

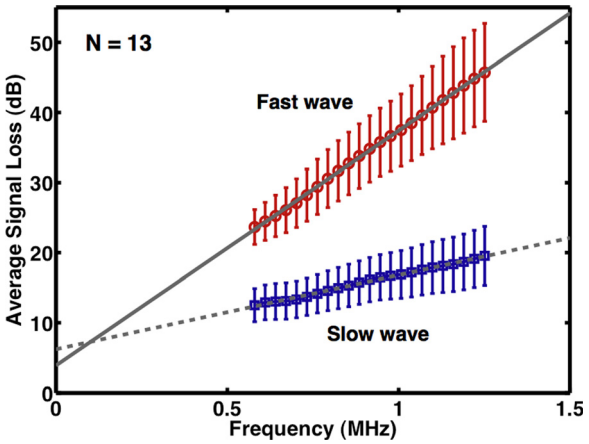

FIG. 3. (Color online) Average ± one standard deviation signal loss of the fast waves and slow waves over 13 sample lengths ranging from $d = 6.0$ mm to 11.8 mm determined using conventional analysis methods. Also displayed are the linear fits over the usable bandwidth. In principle, the zero-frequency intercepts of the linear fits represent the insertion losses of the fast and slow waves.

$$\mathrm{CV(RMSD)} = \frac{\sqrt{\dfrac{\sum_{i=1}^{i=n}\left(x_{\mathrm{data},i} - x_{\mathrm{model},i}\right)^2}{n}}}{\bar{x}_{\mathrm{data}}}, \tag{7}$$

was calculated at each sample thickness. It was observed that the Bayesian algorithm provided better fits to the experimental signals from the thicker samples than the signals obtained from the thinner samples. For sample lengths $\geq$3.5 mm, the CV of the RMSD was approximately constant, suggesting that the Bayesian algorithm achieved reliable separation of the fast and slow waves. However, for sample thicknesses $<$3.5 mm, the CV (RMSD) increased by $\sim$200%. There are several potential explanations for this decrease in the quality of the Bayesian fit. One aspect of this is the presence of higher frequency components in the reference signal. At shorter sample lengths, these high frequency components may still be present in the signal, but their presence is not explicitly accounted for in the propagation model. In contrast, for longer sample lengths, these components have been significantly reduced by the attenuation occurring within the sample. Another aspect is that at thicknesses $<$3.5 mm, the wavelengths of the fast and slow waves are comparable to or larger than the sample thickness. Under those conditions, the current one-dimensional propagation model may not be able to properly characterize the true propagation phenomena and may need to be generalized to a three-dimensional propagation model. A third feature is that at very thin sample lengths, a multiply reflected (within the sample) wave, which has traveled 3 $\times$ d, might interfere with the transmitted wave that has traveled 1 $\times$ d. The current propagation model does not include these reflected fast and slow waves that have traveled 3 $\times$ d. Based on these considerations, the Bayesian estimates for the fast and slow waves are reported for sample thicknesses ranging from 3.5 mm to 11.8 mm, a total of 18 lengths.

E. Comparison of conventional, Bayesian, and MLSP + CF results

Figure 5 shows a comparison of the average signal loss at 1 MHz for the fast and slow waves determined using conventional, Bayesian, and MLSP + CF methods. A study by Wear (2013) found that signal loss, given by

$$\mathrm{SL}_k(f) = A_k \exp\left[-\beta_k f d\right] \tag{8}$$

at the center frequency of the signal, is a more stable parameter than the individual measurements of A_k and β_k. The values shown for all three methods are the average values over sample thicknesses from 6.0 mm to 11.8 mm, even though the Bayesian and MLSP + CF techniques permitted reliable parameter estimates down to the thickness of 3.5 mm. For both the fast wave and slow wave, the Bayesian-estimated and MLSP + CF-estimated values for signal loss agreed quite well with the signal loss determined using conventional analysis. The difference in the average value for signal loss between the Bayesian method and the conventional method was 1.3 dB (3.6%) for the fast wave and only 0.03 dB (0.2%) for the slow wave. Similar values were found for the MLSP + CF method.

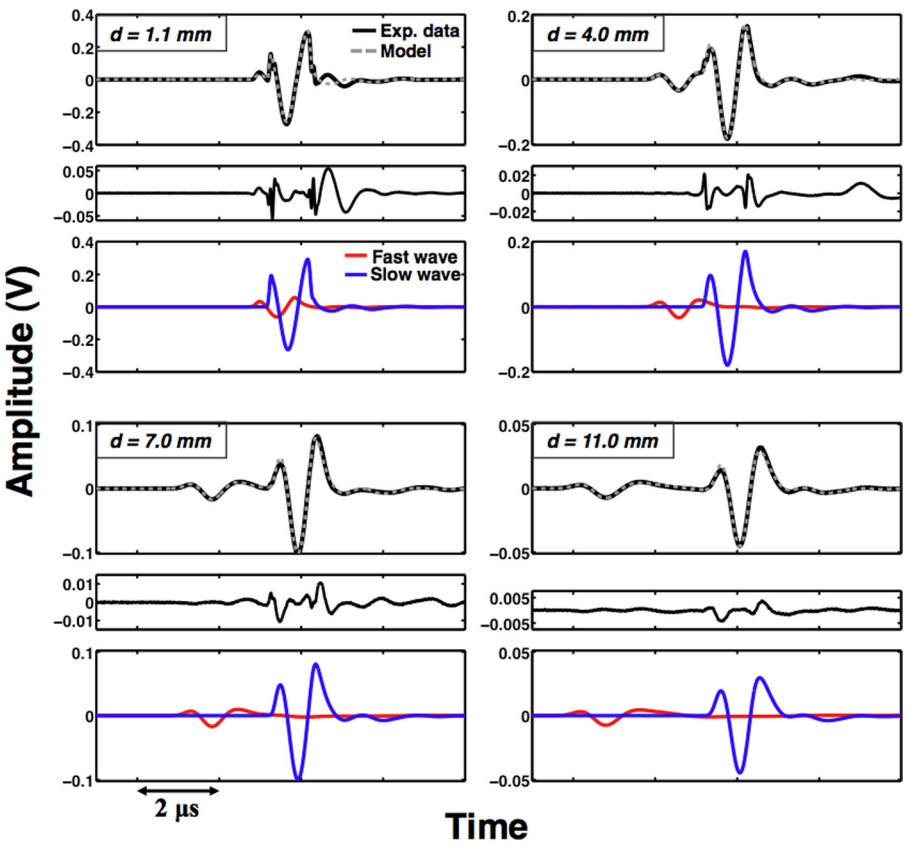

FIG. 4. (Color online) Model results constructed using the parameters estimated from Bayesian probability theory for four representative thicknesses of the equine sample. For each sample thickness: the top panel shows the experimental data along with the model constructed from the Bayesian estimates, the middle panel shows the residual or difference between the data and model, and the bottom panel shows the individual fast and slow waves that make up the model signal. In each panel, the vertical scale was adjusted to facilitate visualizing the signals.

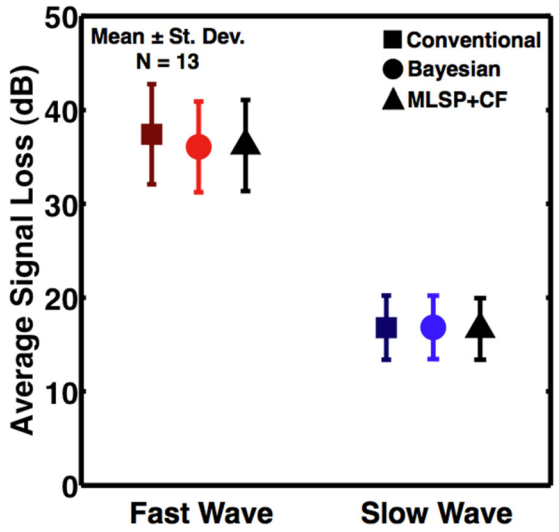

FIG. 5. (Color online) Comparison of the average (±one standard deviation) signal loss at the center frequency (1 MHz) for the fast wave and slow wave using conventional analysis (squares), Bayesian parameter estimation (circles), and MLSP+CF (triangles) over sample thicknesses ranging from 6.0 mm to 11.8 mm ($N = 13$).

Table II displays a comparison of the average fast and slow wave parameters determined by the three methods of analysis. Very good agreement among the three methods was observed for the phase velocity, nBUA, and amplitude, A, of the slow wave. The differences in the average values between conventional and Bayesian analysis methods for the slow wave were 1.5 m/s (0.1%) for the phase velocity, 0.45 dB/cm/MHz (3.9%) for the nBUA, and 0.02 (5.1%) for the A term.

The Bayesian-estimated average phase velocity for the fast wave also agreed quite well with the average phase velocity determined using conventional phase spectroscopy with a difference of 6.2 m/s (0.3%). The MLSP + CF-estimated average phase velocity showed a somewhat higher difference of 17.2 m/s (0.7%). The average estimates for the nBUA and A term of the fast wave determined using Bayesian analysis and MLSP + CF methods were significantly different from the average values determined using conventional analysis methods. For both nBUA and A, the Bayesian and MLSP + CF estimated values were smaller than the values determined by conventional techniques. A value of $A = 1$ means that the total input signal is transmitted into and out of the sample with no reflection losses at either boundary. The Bayesian-estimated and MLSP + CF-estimated values for A were smaller than the conventionally derived A, suggesting that the Bayesian and MLSP + CF algorithms estimated more loss at the boundaries than did the conventional method. The Bayesian-estimated and MLSP + CF-estimated values for nBUA were also smaller than the conventionally determined nBUA, suggesting that the Bayesian and MLSP + CF methods estimated that less loss occurred within the sample than for the case of conventional method. Note that the differences in A and nBUA compensated for each other appropriately in order to maintain similar values of signal loss at the center frequency for all three methods.

TABLE II. Comparison of average (± one standard deviation) parameter values obtained using the three methods for sample thicknesses ranging from 11.8 mm to 6.0 mm.

Parameter	Conventional	Bayesian	MLSP + CF
c_{fast} (1 MHz) (m/s)	2412.2 ± 11.8	2418.4 ± 9.7	2429.4 ± 7.6
c_{slow} (1 MHz) (m/s)	1404.8 ± 1.1	1403.4 ± 1.3	1404.9 ± 2.2
β_{fast} (dB/cm/MHz)	37.7 ± 1.4	30.8 ± 0.7	30.6 ± 1.4
β_{slow} (dB/cm/MHz)	11.8 ± 0.6	11.3 ± 0.5	11.1 ± 0.8
A_{fast}	0.65 ± 0.11	0.37 ± 0.03	0.36 ± 0.03
A_{slow}	0.49 ± 0.05	0.47 ± 0.06	0.47 ± 0.06
SL_{fast} (1 MHz) (dB)	37.4 ± 5.3	36.1 ± 4.8	36.2 ± 4.9
SL_{slow} (1 MHz) (dB)	16.8 ± 3.4	16.8 ± 3.4	16.7 ± 3.3

IV. DISCUSSION

In this study, the phase velocity and attenuation properties of fast and slow waves were measured in a systematically shortened equine cancellous bone specimen using conventional frequency-domain methods, a Bayesian probability theory method, and the MLSP + CF method. However, in many experimental situations with cancellous bone, conventional analysis methods cannot be employed due to the strong overlap of fast and slow waves in both time and frequency domains. In the current study, conventional analysis could not be used for sample lengths under 6.0 mm. In contrast, Bayesian probability theory and MLSP + CF methods were able to estimate the fast and slow wave ultrasonic parameters for almost all sample lengths. For sample lengths that were sufficiently long as to permit conventional analysis, all three techniques yielded comparable values for the phase velocities and signal losses of the fast and slow waves. Therefore, this study demonstrates that the Bayesian probability theory approach and the MLSP + CF method yield reliable estimates of fast and slow wave parameters that are consistent with those determined by conventional techniques and, additionally, can successfully isolate fast and slow waves in cases of significant temporal overlap when conventional methods cannot be applied.

Although the three methods can be used to evaluate similar parameters, there are fundamental differences among them that may lead to disparities in their results. Conventional and MLSP + CF analysis are carried out entirely in the frequency domain, whereas the Bayesian algorithm does the comparison of the model-generated wave and the experimental wave in the time-domain. Additionally, the frequency bands used in the analysis may be different among the three approaches since the frequency range is not restricted to a certain bandwidth in the Bayesian algorithm. The Bayesian and MLSP + CF approaches also assume that the attenuation coefficient and the phase velocity are related by the relationship in Eq. (3), which could lead to errors in the phase velocity/dispersion if the attenuation coefficient is not linear with frequency. The value of A for conventional analysis was determined by extrapolating the signal loss to zero frequency, which is significantly outside the frequency bandwidth of the measurement. Therefore, small errors in the slope of the linear fit of the signal loss over the usable

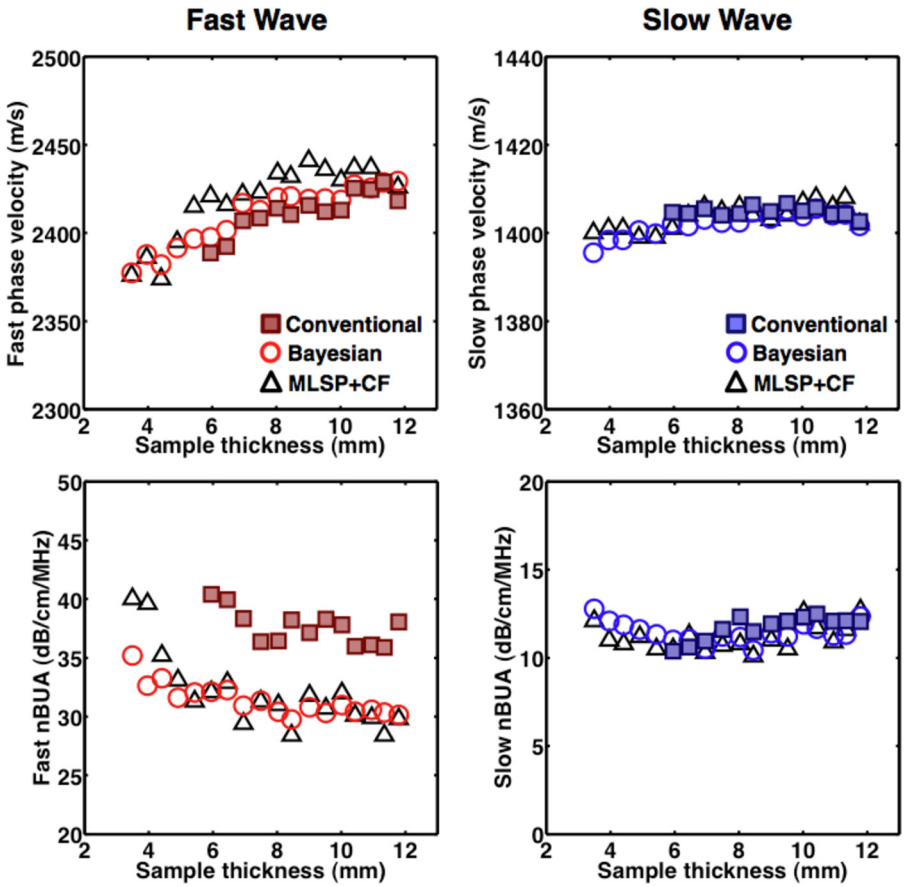

FIG. 6. (Color online) Measurements of phase velocity (at 1 MHz) and nBUA determined using conventional analysis methods, Bayesian analysis methods, and MLSP+CF as functions of sample thickness for fast waves (left column) and slow waves (right column).

frequency range may result in much larger errors in the estimate of A.

A. Trends with sample thickness

In a homogeneous medium that is thick enough so that reverberation effects may be neglected, all six ultrasonic parameters (A_{fast}, A_{slow}, β_{fast}, β_{slow}, $c_{\text{fast}}(f_0)$, $c_{\text{slow}}(f_0)$) should be approximately constant with sample thickness because they are intrinsic properties of the material. Although some variation is to be expected because trabecular bone is heterogeneous, relatively small, systematic changes with sample length were observed, as shown in Fig. 6 for measurements of phase velocity (at 1 MHz) and the slope of the attenuation coefficient (nBUA). While the ultrasonic properties of the slow wave showed little dependence as a function of sample thickness, the properties of the fast wave displayed systematic, almost linear trends with sample thickness. Micro-CT measurements on this equine bone sample revealed a relatively consistent bone volume fraction throughout the specimen. Similar trends with sample thickness for all the fast and slow wave parameters were observed for the three analysis methods studied. For four of the six parameters (A_{slow}, β_{slow}, c_{fast}, c_{slow}), the three methods agreed very well. For the other two parameters (A_{fast}, β_{fast}), there was a discrepancy between the conventional results and the other two methods, which was also observed in the average values shown in Table II. However, when the signal loss at 1 MHz of the fast wave was calculated using Eq. (8) for each sample thickness, the three analysis methods agreed fairly well, as seen in Fig. 7. This is because the signal loss takes into account both the losses occurring within the sample, which are described by the nBUA term, and the losses occurring at the front and back boundaries, which are described by the A term. The discrepancies in A_{fast} and β_{fast} observed among the methods suggest that the analysis methods distribute total signal losses between surface losses (A_{fast}) and bulk losses (β_{fast}) in slightly different proportions. Since A is an extrapolation of signal loss to zero frequency, which is far outside the

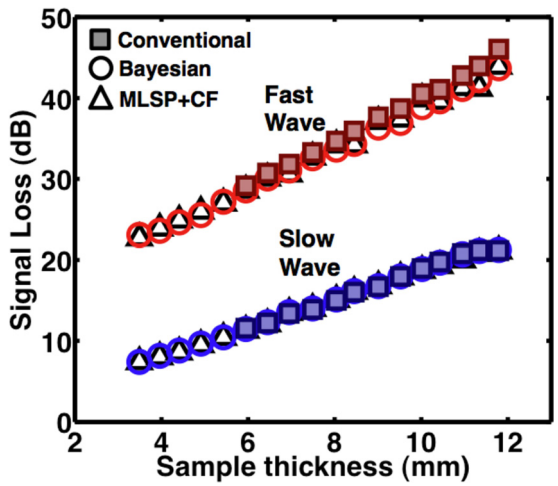

FIG. 7. (Color online) Comparison of the signal loss at 1 MHz for the fast wave and slow wave using conventional analysis (squares), Bayesian parameter estimation (circles), and MLSP+CF (triangles) as a function of sample thickness.

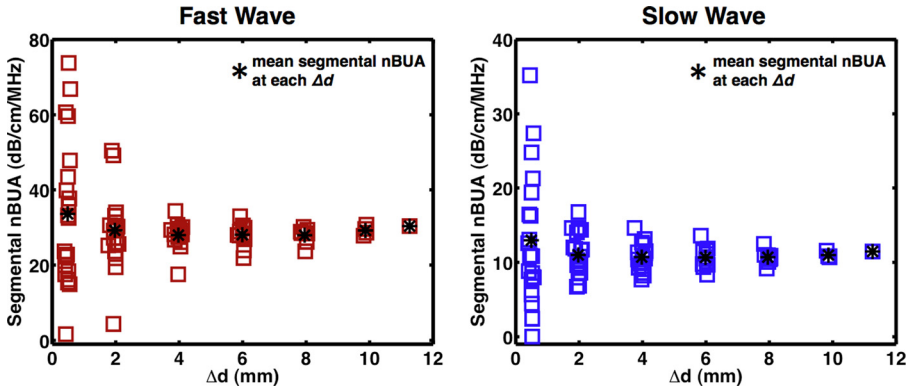

FIG. 8. (Color online) Segmental slopes of the attenuation coefficient (nBUA) of the fast waves (left) and slow waves (right) for $\Delta d = 0.5$ mm, 2 mm, 4 mm, 6 mm, 8 mm, 10 mm, and 11 mm. The stars show the mean nBUA for each value of Δd. As the thickness, Δd, of the segment increases, the estimate of the nBUA appears to improve. Note the change in scale for the slow wave nBUA.

measurement band of frequencies, signal loss at the center frequency may be a more meaningful and stable measurement than A. As expected, the signal loss at the center frequency for both fast and slow waves increased linearly with sample thickness since signal loss is not normalized by bone thickness.

Similar trends with sample thickness were observed in measurements of phase velocity and signal loss of the fast and slow waves in bovine cancellous bone by Wear *et al.* (2014). In the Wear *et al.* (2014) study, two alternative algorithms to the Bayesian algorithm (MLSP + CF and bandlimited deconvolution) were employed to separate fast and slow waves. Since similar trends with sample thickness occurred for the three different methods, this may indicate that the observed trends are not simply artifacts caused by the estimation algorithms. However, the two-mode propagation models used both in this study and in Wear *et al.* (2014) are quite similar, and it is possible that the models are not properly accounting for all the experimental factors. Possible contributions for the systematic dependences on sample length that are not explicitly taken into account in the model include diffraction effects (Xu and Kaufman, 1993; Kaufman *et al.*, 1995), phase cancellation at the face of the finite aperture phase-sensitive receiving transducer (Langton and Subhan, 2001; Bauer *et al.*, 2007; Wear, 2007; Wear, 2008; Cheng *et al.*, 2011), refraction artifacts, and multipath interference.

B. Segmental attenuation

In Fujita *et al.* (2013) and in other studies (Nagatani *et al.*, 2008; Nelson *et al.*, 2011), the reported attenuation properties of the fast and slow waves were for thin slabs, or segments, of the bone sample instead of for the entire bulk of the bone specimen, as was employed in this study. In both Fujita *et al.* (2013) and Nagatani *et al.* (2008), a time-domain method comparing the peak amplitudes of the fast and slow waves for successive sample thickness was employed to determine the apparent (segmental) attenuation for the fast and slow waves. However, it was shown in Nelson *et al.* (2011) that applying time-domain analysis methods to broadband signals may introduce a small sample thickness dependence to the attenuation coefficient, and that frequency domain analysis applied to completely separated fast and slow waves was the least susceptible to sample-thickness-dependent artifacts.

In this study, the segmental attenuations of the fast and slow waves were carried out on the Bayesian-separated fast and slow waves obtained at each sample thickness. This analysis method is a combination of the conventional analysis detailed above (because it occurs in the frequency-domain) and the Fujita *et al.* (2013) time-domain attenuation analysis (because it compares the loss at successive sample thicknesses). The segmental attenuation coefficient is given by

$$\alpha_{\text{seg}}(f) = \frac{\left[10\log\left(|\tilde{V}_n(f)|^2\right) - 10\log\left(|\tilde{V}_{n+1}(f)|^2\right)\right]}{\Delta d}, \tag{9}$$

where $|\tilde{V}(f)|$ are the magnitudes of the Fourier transforms for sample thicknesses corresponding to length indices n and $n+1$, and Δd is the difference between those sample lengths. Segmental attenuation coefficients were determined for combinations of $\Delta d = 0.5$ mm, 2 mm, 4 mm, 6 mm, 8 mm, 10 mm, and 11 mm. At $\Delta d = 8$ mm, for example, there are eight combinations of sample lengths that yield values of the segmental attenuation coefficient given by Eq. (9). The $\Delta d = 11$ mm segmental attenuation coefficients compared the longest and the shortest sample lengths. For both the fast and slow waves, the segmental attenuation varied dramatically with sample length position for small values of Δd. These large variations in the segmental attenuation might be due to actual inhomogeneities in the bone sample, but may be artifacts caused by uncertainties in the sample lengths. However, as Δd became larger, the segmental attenuation coefficients of both fast and slow waves became more consistent. In spite of these variations, the average within any one Δd produced a value for the attenuation coefficient that was in good agreement with the segmental attenuation coefficient averaged over all Δd s. This was also true for the slope of the segmental attenuation coefficient (segmental nBUA) as shown in Fig. 8.

V. CONCLUSION

Conventional, Bayesian, and MLSP + CF analysis methods yielded comparable results for the ultrasonic properties of fast and slow waves in equine cancellous bone. The Bayesian probability theory approach and the MLSP + CF method were able to separate the fast and slow waves and provide reasonable estimates of the fast and slow wave properties even when the waves overlapped in the time and frequency

domains, thus, not permitting application of conventional analysis methods. The Bayesian and MLSP + CF methods provided consistent results even though the former is a time-domain algorithm while the latter is a frequency-domain algorithm and the two methods are predicated on different assumptions. This consistency reinforces confidence in both methods. These algorithms offer useful tools for investigating mechanisms underlying the interaction between ultrasound and poro-elastic media, such as cancellous bone.

ACKNOWLEDGMENTS

This study was supported, in part, by NIH Grant No. R01 AR057433, NIH Grant No. R01 HL040302, and by the Regional Innovation Strategy Support Program of the Ministry of Education, Culture, Sports, and Technology, Japan, and a Grant-in Aid for Scientific Research (B) from the Japan Society for Promotion of Science.

Anderson, C. C., Bauer, A. Q., Holland, M. R., Pakula, M., Laugier, P., Bretthorst, G. L., and Miller, J. G. (**2010**). "Inverse problems in cancellous bone: Estimation of the ultrasonic properties of fast and slow waves using Bayesian probability theory," J. Acoust. Soc. Am. **128**, 2940–2948.

Anderson, C. C., Marutyan, K. R., Holland, M. R., Wear, K. A., and Miller, J. G. (**2008**). "Interference between wave modes may contribute to the apparent negative dispersion observed in cancellous bone," J. Acoust. Soc. Am. **124**, 1781–1789.

Bauer, A. Q., Anderson, C. C., Holland, M. R., and Miller, J. G. (**2009**). "Bone sonometry: Reducing phase aberration to improve estimates of broadband ultrasonic attenuation," J. Acoust. Soc. Am. **125**(1), 522–529.

Bauer, A. Q., Marutyan, K. R., Holland, M. R., and Miller, J. G. (**2007**). "Is the Kramers–Kronig relationship between ultrasonic attenuation and dispersion maintained in the presence of apparent losses due to phase cancellation?," J. Acoust. Soc. Am. **122**, 222–228.

Bauer, A. Q., Marutyan, K. R., Holland, M. R., and Miller, J. G. (**2008**). "Negative dispersion in bone: The role of interference in measurements of the apparent phase velocity of two temporally overlapping signals," J. Acoust. Soc. Am. **123**(4), 2407–2414.

Biot, M. (**1956a**). "Theory of propagation of elastic waves in a fluid-saturated porous solid. I. Low-frequency range," J. Acoust. Soc. Am. **28**, 168–178.

Biot, M. (**1956b**). "Theory of propagation of elastic waves in a fluid-saturated porous solid. II. Higher frequency range," J. Acoust. Soc. Am. **28**, 179–191.

Cardoso, L., Teboul, F., Sedel, L., Oddou, C., and Meunier, A. (**2003**). "In vitro acoustic waves propagation in human and bovine cancellous bone," J. Bone Miner. Res. **18**, 1803–1812.

Cheng, J., Serra-Hsu, F. S., Tian, Y., Lin, W., and Qin, Y. X. (**2011**). "Effects of phase cancellation and receiver aperture size on broadband ultrasonic attenuation for trabecular bone in vitro," Ultrasound Med. Biol. **37**, 2116–2125.

Dencks, S., Barkmann, R., Gluer, C. C., and Schmitz, G. (**2009**). "Model-based parameter estimation in the frequency domain for quantitative ultrasound measurement of bone," in *Proceedings of the IEEE International Ultrasonics Symposium*, pp. 554–557.

Dencks, S., and Schmitz, G. (**2013**). "Estimation of multipath transmission parameters for quantitative ultrasound measurements of bone," IEEE Trans. Ultrason. Ferroelectr. Freq. Control **60**, 1884–1895.

Fellah, Z. E. A., Chapelon, J. Y., Berger, S., Lauriks, W., and Depollier, C. (**2004**). "Ultrasonic wave propagation in human cancellous bone: Application of Biot theory," J. Acoust. Soc. Am. **116**, 61–73.

Fujita, F., Mizuno, K., and Matsukawa, M. (**2013**). "An experimental study on the ultrasonic wave propagation in cancellous bone: Waveform changes during propagation," J. Acoust. Soc. Am. **134**(6), 4775–4781.

Haire, T. J., and Langton, C. M. (**1999**). "Biot theory: A review of its application to ultrasound propagation through cancellous bone," Bone **24**, 291–295.

Hasegawa, S., Nagatani, Y., Mizuno, K., and Matsukawa, M. (**2010**). "Wavelet transform analysis of ultrasonic wave propagation in cancellous bone," Jpn. J. Appl. Phys. **49**, 07HF28.

Hoffman, J. J., Nelson, A. M., Holland, M. R., and Miller, J. G. (**2012**). "Cancellous bone fast and slow waves obtained with Bayesian probability theory correlate with porosity from computed tomography," J. Acoust. Soc. Am. **132**, 1830–1837.

Hosokawa, A., and Otani, T. (**1997**). "Ultrasonic wave propagation in bovine cancellous bone," J. Acoust. Soc. Am. **101**, 558–562.

Hosokawa, A., and Otani, T. (**1998**). "Acoustic anisotropy in bovine cancellous bone," J. Acoust. Soc. Am. **103**, 2718–2722.

Hughes, E. R., Leighton, T. G., White, P. R., and Petley, G. W. (**2007**). "Investigation of an anisotropic tortuosity in a Biot model of ultrasonic propagation in cancellous bone," J. Acoust. Soc. Am. **121**, 568–574.

Kaufman, J., Xu, W., Chiabrera, A., and Siffert, R. (**1995**). "Diffraction effects in insertion mode estimation of ultrasonic group velocity," IEEE Trans. Ultrason. Ferroelectr. Freq. Control **42**(2), 232–242.

Langton, C. M., and Subhan, M. (**2001**). "Computer and experimental simulation of a cortical end-plate phase cancellation artifact in the measurement of BUA at the calcaneus," Physiol. Meas. **22**, 581–587.

Lashkari, B., Manbachi, A., Mandelis, A., and Cobbold, R. S. C. (**2012**). "Slow and fast ultrasonic wave detection improvement in human trabecular bones using Golay code modulation," J. Acoust. Soc. Am. **132**(3), EL222–EL228.

Laugier, P., and Haïat, G. (Eds.) (**2011**). *Bone Quantitative Ultrasound* (Springer, Netherlands), Chap. 3, pp. 47–71.

Lee, K. I., Hughes, E. R., Humphrey, V. F., Leighton, T. G., and Choi, M. J. (**2007**). "Empirical angle-dependent Biot and MBA models for acoustic anisotropy in cancellous bone," Phys. Med. Biol. **52**, 59–73.

Maruo, S., and Hosokawa, A. (**2014**). "A generalized harmonic analysis of ultrasound waves propagating in cancellous bone," Jpn. J. Appl. Phys. **53**, 07KF06.

Marutyan, K. R., Bretthorst, G. L., and Miller, J. G. (**2007**). "Bayesian estimation of the underlying bone properties from mixed fast and slow mode ultrasonic signals," J. Acoust. Soc. Am. **121**, EL8–EL15.

Marutyan, K. R., Holland, M. R., and Miller, J. G. (**2006**). "Anomalous negative dispersion in bone can result from the interference of fast and slow waves," J. Acoust. Soc. Am. **120**, EL55–EL61.

Mizuno, K., Matsukawa, M., Otani, T., Takada, M., Mano, I., and Tsujimoto, T. (**2008**). "Effects of structural anisotropy of cancellous bone on speed of ultrasonic fast waves in the bovine femur," IEEE Trans. Ultrason. Ferroelectr. Freq. Control **55**, 1480–1487.

Nagatani, Y., Mizuno, K., Saeki, T., Matsukawa, M., Sakaguchi, T., and Hosoi, H. (**2008**). "Numerical and experimental study on the wave attenuation in bone—FDTD simulation of ultrasound propagation in cancellous bone," Ultrasonics **48**, 607–612.

Nagatani, Y., and Tachibana, R. O. (**2014**). "Multichannel instantaneous frequency analysis of ultrasound propagating in cancellous bone," J. Acoust. Soc. Am. **135**, 1197–1206.

Nelson, A. M., Hoffman, J. J., Anderson, C. C., Holland, M. R., Nagatani, Y., Mizuno, K., Matsukawa, M., and Miller, J. G. (**2011**). "Determining attenuation properties of interfering fast and slow ultrasonic waves in cancellous bone," J. Acoust. Soc. Am. **130**, 2233–2240.

Njeh, C. F., Hans, D., Fuerst, T., Gluer, C. C., and Genant, H. K. (Eds.) (**1999**). *Quantitative Ultrasound: Assessment of Osteoporosis and Bone Status* (Martin Dunitz, London), Chap. 4, pp. 67–77.

O'Donnell, M., Jaynes, E. T., and Miller, J. G. (**1981**). "Kramers–Kronig relationship between ultrasonic attenuation and phase velocity," J. Acoust. Soc. Am. **69**, 696–701.

Ophir, J., and Jaeger, P. (**1982**). "Spectral shifts of ultrasonic propagation through media with nonlinear dispersive attenuation," Ultrason. Imaging **4**, 282–289.

Waters, K., and Hoffmeister, B. K. (**2005**). "Kramers–Kronig analysis of attenuation and dispersion in trabecular bone," J. Acoust. Soc. Am. **118**, 3912–3920.

Waters, K., Hughes, M., Mobley, J., and Miller, J. (**2003**). "Differential forms of the Kramers–Kronig dispersion relations," IEEE Trans. Ultrason. Ferroelectr. Freq. Control **50**, 68–76.

Waters, K. R., Mobley, J., and Miller, J. G. (**2005**). "Causality-imposed (Kramers–Kronig) relationships between attenuation and dispersion," IEEE Trans. Ultrason. Ferroelectr. Freq. Control **52**, 822–833.

Wear, K. A. (**2007**). "The effect of phase cancellation on estimates of calcaneal broadband ultrasound attenuation in vivo," IEEE Trans. Ultrason. Ferroelectr. Freq. Control **54**, 1352–1359.

Wear, K. A. (**2008**). "The effect of phase cancellation on estimates of broadband ultrasound attenuation and backscatter coefficient in human

calcaneus in vitro," IEEE Trans Ultrason. Ferroelectr. Freq. Control **55**, 384–390.
Wear, K. A. (**2010**). "Decomposition of two-component ultrasound pulses in cancellous bone using modified least squares Prony's method—Phantom experiment and simulation," Ultrasound Med. Biol. **36**, 276–287.
Wear, K. A. (**2013**). "Estimation of fast and slow wave properties in cancellous bone using Prony's method and curve fitting," J. Acoust. Soc. Am. **133**, 2490–2501.
Wear, K. A. (**2014**). "Time-domain separation of interfering waves in cancellous bone using bandlimited deconvolution: Simulation and phantom study," J. Acoust. Soc. Am. **135**, 2102–2112.
Wear, K. A., Nagatani, Y., Mizuno, K., and Matsukawa, M. (**2014**). "Fast and slow wave detection in bovine cancellous bone in vitro using bandlimited deconvolution and Prony's method," J. Acoust. Soc. Am. **136**(4), 2015–2024.
Xu, W., and Kaufman, J. (**1993**). "Diffraction correction methods for insertion ultrasound attenuation estimation," IEEE Trans. Biomed. Eng. **40**(6), 563–570.